The Science Case for Spacecraft Exploration of the Uranian Satellites: Candidate Ocean Worlds in an Ice Giant System

Richard J. Cartwright[1,10] , Chloe B. Beddingfield[1,2] , Tom A. Nordheim[3] , Catherine M. Elder[3] , Julie C. Castillo-Rogez[3] , Marc Neveu[4] , Ali M. Bramson[5] , Michael M. Sori[5] , Bonnie J. Buratti[3] , Robert T. Pappalardo[3] , Joseph E. Roser[1,2] , Ian J. Cohen[6] , Erin J. Leonard[3] , Anton I. Ermakov[7] , Mark R. Showalter[1] , William M. Grundy[8,9] , Elizabeth P. Turtle[6] , and Mark D. Hofstadter[3]

[1] The Carl Sagan Center at the SETI Institute, 189 Bernardo Avenue, Suite 200, Mountain View, CA 94043, USA; rcartwright@seti.org
[2] NASA Ames Research Center, Building N245, Room 204, Moffett Field, CA 94035, USA
[3] Jet Propulsion Laboratory, California Institute of Technology, 4800 Oak Grove Drive, Pasadena, CA 91109, USA
[4] NASA Goddard Space Flight Center, 8800 Greenbelt Road, Greenbelt, MD 20771, USA
[5] Purdue University, 610 Purdue Hall, West Lafayette, IN 47907, USA
[6] John Hopkins University Applied Physics Laboratory, 11100 John Hopkins Road, Laurel, MD 20723, USA
[7] University of California, Berkeley 2200 University Avenue, Berkeley, CA 94720, USA
[8] Lowell Observatory, 1400 W Mars Hill Road, Flagstaff, AZ 86001, USA
[9] Northern Arizona University, S San Francisco Street, Flagstaff, AZ 86011, USA

Abstract

The 27 satellites of Uranus are enigmatic, with dark surfaces coated by material that could be rich in organics. Voyager 2 imaged the southern hemispheres of Uranus's five largest "classical" moons—Miranda, Ariel, Umbriel, Titania, and Oberon, as well as the largest ring moon, Puck—but their northern hemispheres were largely unobservable at the time of the flyby and were not imaged. Additionally, no spatially resolved data sets exist for the other 21 known moons, and their surface properties are essentially unknown. Because Voyager 2 was not equipped with a near-infrared mapping spectrometer, our knowledge of the Uranian moons' surface compositions, and the processes that modify them, is limited to disk-integrated data sets collected by ground- and space-based telescopes. Nevertheless, images collected by the Imaging Science System on Voyager 2 and reflectance spectra collected by telescope facilities indicate that the five classical moons are candidate ocean worlds that might currently have, or had, liquid subsurface layers beneath their icy surfaces. To determine whether these moons are ocean worlds, and to investigate Uranus's ring moons and irregular satellites, close-up observations and measurements made by instruments on board a Uranus orbiter are needed.

1. Introduction and Rationale for a Spacecraft Mission to Uranus

The surfaces of Uranus's large and tidally locked "classical" moons—Miranda, Ariel, Umbriel, Titania, and Oberon—exhibit widespread photogeologic evidence for endogenic activity. The ubiquitous evidence hinting at geologic communication between the interiors and surfaces of these moons, in particular on Miranda and Ariel, makes them candidate ocean worlds that may have, or once had, subsurface liquid H_2O layers beneath their icy exteriors (Hendrix et al. 2019; Beddingfield & Cartwright 2020b; Schenk & Moore 2020). In 1986, the Voyager 2 spacecraft flew by the Uranian system and collected tantalizing snapshots of these classical moons, measured Uranus's offset and tilted magnetic field, and discovered ten new ring moons orbiting within Uranus's ring system (e.g., Smith et al. 1986). Since this brief flyby, exploration of Uranus and its satellites has remained in the purview of ground- and space-based telescopes. At near-infrared

(NIR) wavelengths, these telescope observations have revealed that the surfaces of the five classical moons are dominated by H_2O ice mixed with dark material that could be rich in organics and silicate minerals (e.g., Cruikshank et al. 1977; Cruikshank 1980; Cruikshank & Brown 1981; Soifer et al. 1981; Brown & Cruikshank 1983; Brown & Clark 1984). NIR observations have also detected carbon dioxide (CO_2) ice on the classical moons (Grundy et al. 2003, 2006; Cartwright et al. 2015), and nitrogen-bearing constituents like ammonia (NH_3) and ammonium (NH_4^+) could be present in surface deposits as well (Bauer et al. 2002; Cartwright et al. 2018; Cook et al. 2018; Cartwright et al. 2020c; DeColibus et al. 2020). The surfaces of the classical moons could therefore be rich in C, H, O, and N-bearing species, representing some of the key chemical requirements for life as we know it.

Although data collected by Voyager 2 and ground- and space-based telescope facilities have led to some fascinating discoveries, our understanding of Uranus's classical moons is severely limited by the absence of data collected during close-up observations made by a Uranus orbiter. Similarly, Uranus's small ring moons and irregular satellites remain unexplored, and their surface geologies and compositions are almost entirely unknown. New measurements made by modern instruments on board an orbiting spacecraft are critical to investigate the surfaces and interiors of the classical moons and determine whether they are ocean worlds with present day subsurface liquid H_2O layers. As described by multiple recent studies (e.g., Fletcher et al. 2020; Cohen et al. 2020;

Table 1
Science Drivers for the Exploration of the Uranian System with an Orbiter

Science Questions	Observations and Measurements	Instruments
• Do the classical moons have subsurface oceans that could harbor life, either now or in the past? • Is there active geologic communication between the classical moons' surfaces and interiors?	• Search for induced magnetic fields, plumes, hot spots, and cryovolcanic features. • Search for surface changes since the Voyager 2 flyby. • Capture dust samples from active plumes (if present).	Magnetometer VIS camera MIR camera VIS/NIR mapping spectrometer Dust spectrometer
• What geologic processes have modified the surfaces of the classical moons?	• Characterize the morphology, topography, and composition of geologic features and terrains on their surfaces. • Measure impact crater densities.	VIS camera VIS/NIR mapping spectrometer
• Do the classical moons have tenuous atmospheres? • Do volatile constituents migrate seasonally?	• Search for exospheres. • Characterize the distributions and spectral signatures of condensed volatiles.	VIS camera VIS/NIR mapping spectrometer Plasma spectrometer UV imaging spectrometer
• Do magnetospheric charged particles weather the surfaces of the ring moons and classical moons?	• Characterize magnetic field and charged particle populations proximal to these moons. • Search for evidence of irradiation darkening of surface ices and the presence of radiolytic products.	Magnetometer Plasma spectrometer Energetic particle detector VIS/NIR mapping spectrometer UV imaging spectrometer
• Is the red material on the classical moons organic-rich, and did it originate from the irregular satellites?	• Make an inbound flyby of an irregular satellite, and image the irregular satellites while in Uranus orbit. • Characterize the compositions of the classical moons and collect dust samples.	VIS camera VIS/NIR mapping spectrometer Dust spectrometer
• Does the ring moon Mab sustain the μ-ring? • Does μ-ring material coat Puck and Miranda?	• Compare the surface compositions of Puck and Miranda to the composition of Mab and the μ-ring. • Collect μ-ring dust samples.	VIS camera VIS/NIR mapping spectrometer Dust spectrometer
• What is the dynamic history of the moons? • Did the classical moons share orbital resonances in the past, and did these resonances drive tidal heating and endogenic activity?	• Measure eccentricities, inclinations, tidal $Q(\omega)$ of Uranus, and Love numbers. Analyze topography of geologic features to estimate paleo heat fluxes.	Radio science subsystem VIS camera
• Did the classical moons form in Uranus's circumplanetary disk or evolve from its rings?	• Measure crater frequency distributions. • Compare surface compositions of ring moons and classical moons. • Search for streamer channels in the rings.	VIS camera VIS/NIR mapping spectrometer

Beddingfield et al. 2020a; Leonard et al. 2021), a mission to Uranus would allow us to study interactions between Uranus's magnetosphere and its rings and moons, improve our understanding of how geologic processes operate in cold and distant ice giant systems, and enable a more complete investigation of organics in the outer solar system. An orbiter would provide us with an unparalleled opportunity to study the origin and evolution of Uranus's ring-moon system. Furthermore, an orbiter could provide new insight into the origins of Uranus's irregular satellites, and whether they were sourced from the primordial Kuiper Belt or were captured from nearby heliocentric orbits (e.g., Jewitt & Haghighipour 2007

Multiple close proximity flybys made by a Uranus orbiter would therefore address many outstanding science questions for the Uranian system (Table 1). A spacecraft mission to Uranus can be carried out with existing chemical propulsion technology by making use of a Jupiter gravity assist in the 2030–2034 time frame, leading to a flight time of only ~11 years, arriving in the early to mid 2040s (Hofstadter et al. 2019). Crucially, this arrival time frame in northern summer would allow us to observe the Uranian moons' northern hemispheres, which were shrouded by winter darkness at the time of the Voyager 2 flyby and have never been imaged. An orbiter could then continually collect data and search for evidence of ongoing geologic activity, as well as search for evidence of volatile migration of CO_2 and other species in response to seasonal changes as the Uranian system transitions into southern spring in 2050.

An orbiter equipped with several key instruments could determine whether the classical Uranian moons are ocean worlds. The highest priority instrument for identifying subsurface oceans is a magnetometer, which could detect and characterize induced magnetic fields emanating from briny liquid layers in the interiors of these moons. Visible (VIS;
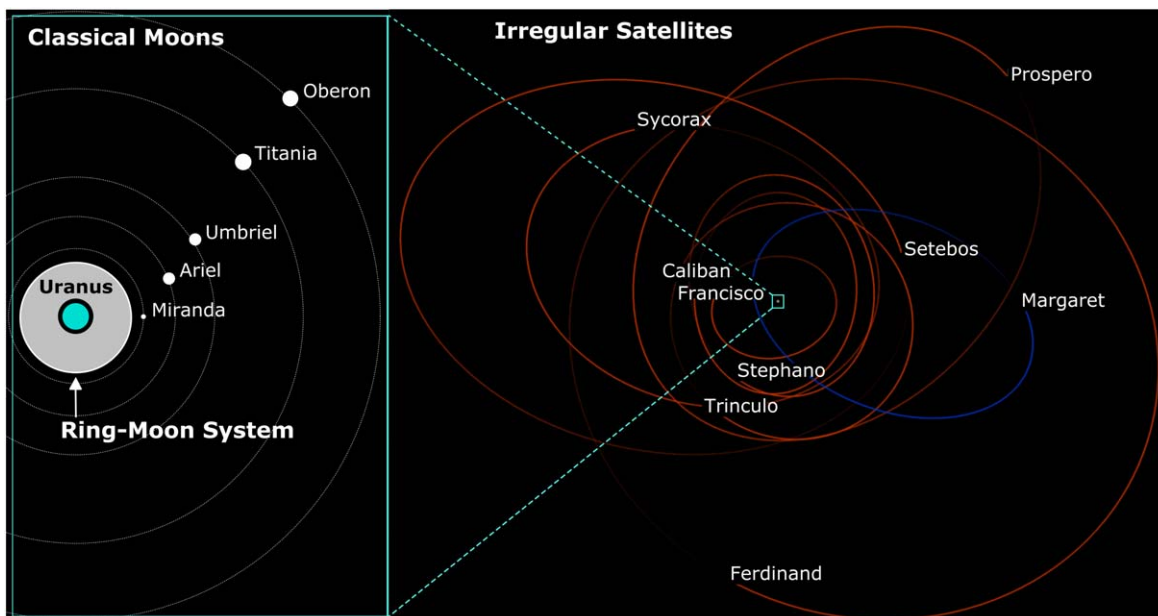
Figure 1. Left: diagram illustrating the orbital zones of the ring moons and the classical moons. The sizes of the five classical moons (white filled circles) are scaled correctly relative to each other, but have been increased by a factor of 20 relative to the size of Uranus (cyan filled circle). The orbits and relative sizes of the ring moons are shown in Figure 3. Right: diagram illustrating the orbits of Uranus's eight retrograde irregular satellites (red) and one prograde irregular satellite (blue). The orbital zone of the ring and classical moons is contained within the cyan colored box. The orbits of the irregular satellites were simulated using orbital elements provided on the Jet Propulsion Laboratory Horizons On-Line Ephemeris System (https://ssd.jpl.nasa.gov/?sat_elem, originally generated by: Nrco0e—Own work, CC BY-SA 4.0, https://commons.wikimedia.org/w/index.php?curid=98634845).

0.4–0.7 μm) and mid-infrared (MIR; 5–250 μm) cameras would be vital for identifying recent geologic activity, hot spots, and possible communication between the interiors and surfaces of these moons. A VIS and NIR mapping spectrometer (0.4–5 μm) would be critical for characterizing the spectral signature and distribution of volatile species that could result from recent outgassing of material, as well as endogenic salts that may have been exposed or emplaced by geologic activity. Ideally, an orbiter would get close enough to achieve spatial resolutions of $\lesssim$100 m/pixel for large regions of each classical moon's surface. If only a limited number of close flybys are possible, Ariel and Miranda likely represent the highest priority targets because they display the best evidence for geologic activity in the recent past.

2. Background and Science Questions

Uranus is orbited by 27 known moons (Figure 1), including its five largest moons, Miranda, Ariel, Umbriel, Titania, and Oberon, which have semimajor axes ranging between 5.1 and 23 Uranian radii (R_U) (Table 2, Figure 2). Interior to the classical moons, 13 small ring moons orbit within Uranus ring system, with semimajor axes ranging between 2 and 3.8 R_U (Table 3 and Figure 3). Far beyond the orbital zone of the classical moons, nine irregular satellites orbit Uranus on highly inclined and eccentric orbits, with semimajor axes ranging between 169 and 806 R_U (Table 3, Figure 1). In the following subsections, we briefly describe the state of knowledge and some of the outstanding science questions for these 27 moons.

2.1. Geology of the Uranian Satellites

Classical moons. The Imaging Science System (ISS) on board Voyager 2 collected fascinating images of the five classical moons (Figure 2). Because the Voyager 2 flyby occurred during southern summer, when the subsolar point was

$\sim$82°S, the northern hemispheres of these moons were mostly hidden from view and were not imaged (Smith et al. 1986). The incomplete spatial coverage, and generally low spatial resolution of the available images, limits our understanding of different terrains and geologic features, in particular for the more distant moons Umbriel, Titania, and Oberon.

The innermost moon Miranda displays abundant evidence for endogenic geologic activity, including three large polygonal shaped regions called coronae, which were likely formed by tectonic and/or cryovolcanic processes (Figures 1(a)–(c)) (e.g., Smith et al. 1986; Croft & Soderblom 1991; Greenberg et al. 1991; Schenk 1991; Kargel 1995; Pappalardo et al. 1997; Hammond & Barr 2014; Beddingfield et al. 2015; Beddingfield & Cartwright 2020b). The origin and timescale of activity on Miranda is not well understood, and it is unknown if this activity is associated with a subsurface ocean, either now or in the past. Searching for and characterizing induced magnetic fields, plumes, and surface heat anomalies, as well as analyzing geologic surface features interpreted to be cryovolcanic in origin, is paramount to determine if Miranda is an ocean world. Tidal heating of Miranda from past orbital resonances (Tittemore & Wisdom 1990; Ćuk et al. 2020) may have been an important driver of resurfacing in the recent past. Additionally, Miranda displays ancient cratered terrain pockmarked with "subdued" craters, which have smooth floors and subtle rims that have been mantled by an unknown source of material (e.g., Smith et al. 1986; Beddingfield & Cartwright 2020b; Cartwright et al. 2020a). These subdued craters are reminiscent of lunar highlands and could be blanketed by impact-generated regolith (Croft 1987), but they are also reminiscent of the plume-mantled craters on the ocean world Enceladus (e.g., Kirchoff & Schenk 2009), hinting that a similar plume-driven mantling process may have occurred on Miranda.

Table 2
Overview of the Five Classical Moons' Geologies and Surface Compositions

Classical Moons	[a]Semimajor Axis (10^5 km)	[a]Mean Radius (km)	Geologic Features and Regions of Interest	Highest Res. Images (km/pix)	Known Surface Constituents	Possible Surface Constituents
Miranda	1.299	235.8 ± 0.7	Polygonal shaped coronae, large scale rift system, populations of subdued and fresh craters.	~0.25	H_2O ice	
Ariel	1.909	578.9 ± 0.6	Large chasmata, flow bands, smooth plains, cratered plains, large lobate shaped features.	~1	H_2O ice CO_2 ice	[b]Organics, [b]hydrated silicates, [c]NH_3 and NH_4 bearing species, [c] carbonates, [d]trapped OH
Umbriel	2.660	584.7 ± 2.8	Heavily cratered surface with some bright-floored craters, polygonal basins.	~5	H_2O ice CO_2 ice	
Titania	4.363	788.9 ± 1.8	Large chasmata, smooth plains, linear features, cratered terrain.	~3	H_2O ice CO_2 ice	
Oberon	5.835	761.4 ± 2.6	Large chasmata, smooth plains, cratered terrain, ~11 km tall mountain.	~6	H_2O ice CO_2 ice	

Notes.
[a] Semimajor axis and mean radius values from the Jet Propulsion Laboratory Horizons On-Line Ephemeris System and references therein (https://ssd.jpl.nasa.gov/?sat_elem).
[b] Possibly contributing to the ubiquitous dark material and spectrally red material observed by Voyager 2.
[c] Possible contributors to a 2.2 μm absorption band detected in some ground-based spectra.
[d] Possibly contributing to a 0.28 μm absorption band detected in Hubble Space Telescope spectra.

Miranda's neighbor, Ariel, also displays widespread evidence for resurfacing that could have been spurred by ocean world activity. Sections of Ariel's imaged surface are dominated by large canyons called "chasmata" (Figure 2(d) and (e)) that were likely formed by tectonic processes (e.g., Smith et al. 1986). The smooth floors of some of these chasmata are bowed up with two parallel medial ridges that are separated by a topographic low, reminiscent of fissure style volcanism on Earth (Schenk 1991). Large fracture systems cut across other parts of Ariel's surface, and clusters of curvilinear features referred to as "flow bands" could be cryovolcanic features (e.g., Plescia 1987; Croft & Soderblom 1991; Schenk 1991; Beddingfield & Cartwright 2021). Furthermore, Ariel's surface geology is consistent with high heat fluxes in its interior, which could drive extrusion of material (Peterson et al. 2015). Some regions of Ariel's surface are relatively young (~1–2 Ga) (Zahnle et al. 2003), but the fairly low resolution of the ISS images ($\gtrsim$1 km/pixel) makes investigation of the processes that formed these younger terrains more difficult.

Although Umbriel has the darkest and oldest surface of the five classical moons (e.g., Smith et al. 1986; Zahnle et al. 2003), it has some large craters with bright floors, like Wunda crater, which has a bright annulus of material surrounding its central peak (e.g., Smith et al. 1986) (Figure 2(f)). Wunda crater is located near the center of Umbriel's trailing hemisphere, where the abundance of CO_2 ice is highest (Grundy et al. 2006; Cartwright et al. 2015). Consequently, the bright annulus of material mantling this crater may represent a large deposit of CO_2 ice, possibly originating from post-impact cryovolcanic infilling (Helfenstein et al. 1989), or from the accumulation of radiolytically produced CO_2 molecules that get cold trapped in Wunda (Sori et al. 2017). Furthermore, large polygonal basins are present on Umbriel, hinting at global-scale resurfacing in the past (Helfenstein et al. 1989).

However, the poor resolution of the available data ($\gtrsim$5 km/pixel) severely limits analyses of these features and our ability to determine whether they resulted from ocean world activity.

The surfaces of the outer moons Titania and Oberon exhibit evidence for tectonism, with large chasmata and linear surface features, as well as smooth plains that may have formed from cryovolcanic processes (e.g., Smith et al. 1986; Croft & Soderblom 1991) (Figures 2(g), (h)). Additionally, Oberon has an ~11 km tall "limb mountain" that could be the central peak for a relaxed complex crater (Smith et al. 1986; McKinnon et al. 1991; Croft & Soderblom 1991; Moore et al. 2004). Similar to Umbriel, the poor resolution of the ISS images for Titania and Oberon ($\gtrsim$3 and 6 km/pixel, respectively) limits our ability to investigate possible ocean world activity on these two moons.

Relatively less is known about the interiors of the classical moons, and measuring magnetic induction with a magnetometer is critical for determining whether they possess subsurface oceans (Cochrane et al. 2021; Weiss et al. 2021). Other measurements are needed to investigate the internal structures and bulk compositions of these moons, which is critical for improving our understanding of their formation and evolution. The densities of Ariel, Umbriel, Titania, and Oberon are 1.66 ± 0.15 g cm^{-3}, 1.39 ± 0.16 g cm^{-3}, 1.71 ± 0.05 g cm^{-3}, and 1.63 ± 0.05 g cm^{-3}, respectively, indicating that these moons are made of at least 50% silicate material by mass, whereas Miranda's density is only 1.2 ± 0.14 g cm^{-3}, indicating a larger H_2O ice fraction (Jacobson et al. 1992). Measuring the non-spherical gravity field would shed light on the differentiation state and the nature of the endogenic activity exhibited by these moons. Measuring libration amplitudes (Steinbrügge et al. 2019) could also be used to investigate whether these moons have subsurface liquid layers. Furthermore, searching for thermal anomalies across the surfaces of these moons, using a MIR camera equipped with a suite of multiple
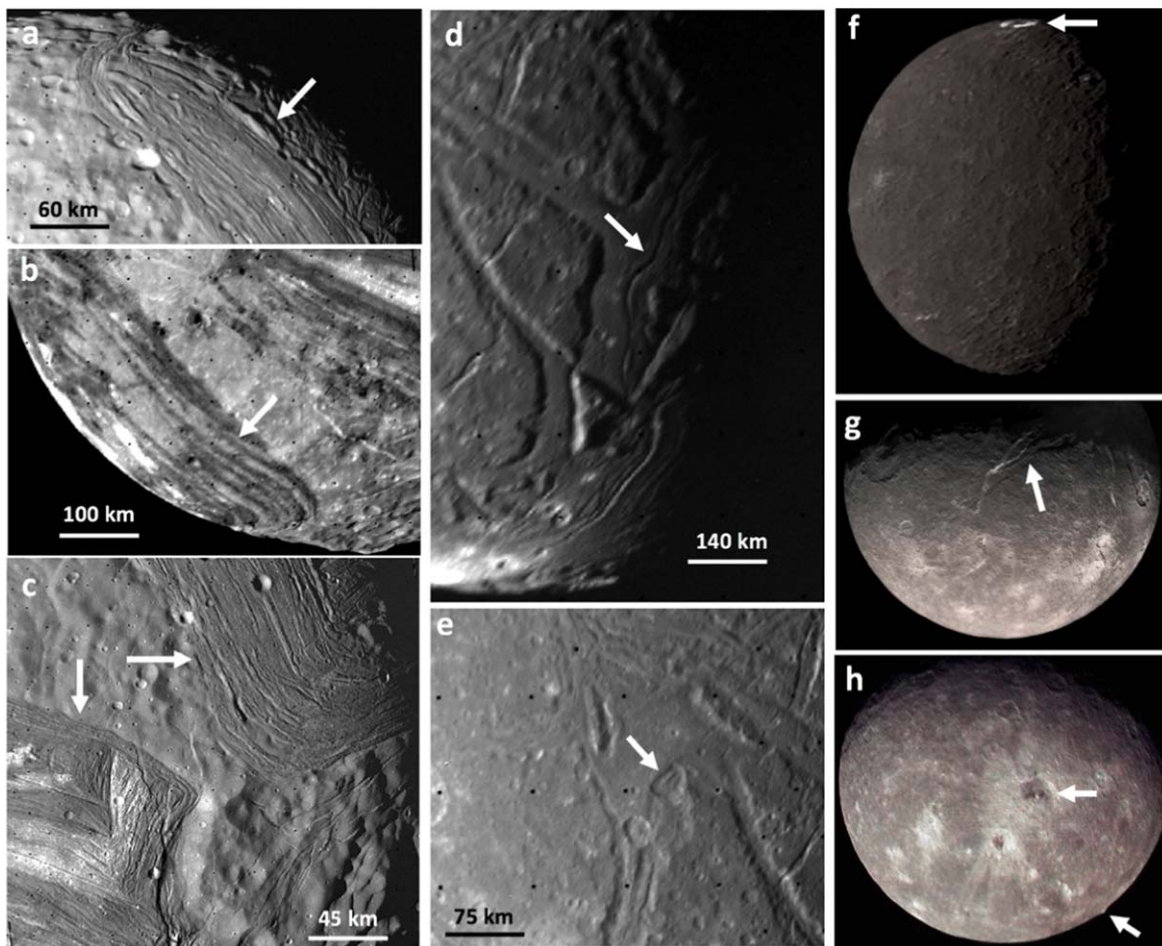
Figure 2. Voyager 2/ISS images of the five classical Uranian moons. White arrows highlight: (a) ridges on Miranda, which possibly have a cryovolcanic and/or tectonic origin (image shows primarily the trailing hemisphere); (b) Arden Corona on Miranda with high and low albedo banding along large tectonic faults (primarily leading hemisphere); (c) Inverness (bottom left) and Elsinore (top right) Coronae on Miranda that exhibit ridges and grooves (image centered near 45°S latitude and 300° longitude). Between these two coronae are examples of craters that have been mantled by an unknown source of material. (d) Large chasmata with medial grooves on Ariel (primarily trailing hemisphere); (e) an impact crater on Ariel, possibly infilled by cryolava (centered near 50°S latitude, 10° longitude). (f) The bright floor of Wunda crater on Umbriel; (g) the large Messina Chasmata on Titania; and (h) the smooth floor of Hamlet crater and an 11 km tall limb mountain on Oberon. The ISS image mosaics in (f)–(h) show both the leading and trailing hemispheres of these three moons, with their south poles located toward the bottom center of each image (reprocessed by Stryk & Stooke 2008). A grid of Reseau points were embedded in images collected by ISS (regular pattern of black-filled circles in (a)–(e)).

narrow and wide filters spanning 5–250 μm, would improve our understanding of their heat budgets and the long-term surviva-bility of liquid water in their interiors. Thus, characterizing the surfaces and interiors of the classical moons to determine whether they are, or were, ocean worlds requires high resolution data sets, which can only be collected by a Uranus orbiter making multiple close flybys of each moon.

Ring moons and irregular satellites. Uranus possesses the most densely packed group of moons in the solar system, with nine ring moons (Bianca to Perdita) orbiting between 59,000 and 77,000 km from the planet's center (e.g., Showalter 2020). Voyager 2 initially discovered 10 ring moons: Cordelia, Ophelia, Bianca, Cressida, Desdemona, Juliet, Portia, Rosalind, Belinda, and Puck (e.g., Smith et al. 1986). Perdita was discovered later through reanalysis of Voyager 2 images (Karkoschka 2001). Cupid and Mab were discovered using the Hubble Space Telescope (Showalter & Lissauer 2006; De Pater et al. 2006). Mab orbits within the outermost and dusty μ-ring (blue colored region in Figure 3), which might be sustained by material ejected from the surface of this tiny moon (De Pater et al. 2006; Showalter & Lissauer 2006; Sfair & Winter 2012). Furthermore, μ-ring material could spiral inward and coat the

leading hemisphere of Puck (French et al. 2017), and perhaps it also spirals outward and mantles Miranda, possibly contribut-ing to its substantial regolith cover (Cartwright et al. 2020a, 2020b). Little is known about the surface geologies of the ring moons as only Puck was spatially resolved by Voyager 2/ISS (~4.5 km/pixel) (Figure 3). These ISS images revealed a heavily cratered surface, suggesting that Puck may have been collisionally disrupted and then reaccreted into a rubble pile (Smith et al. 1986; Croft & Soderblom 1991). Voyager 2 did not detect any of Uranus's nine known irregular satellites, which were discovered by ground-based observers (Gladman et al. 1998, 2000; Kavelaars et al. 2004; Sheppard et al. 2005). Thus, the geologies of Uranus ring moons and irregular satellites remain unexplored, and new observations made by an orbiter would dramatically expand our knowledge of these objects.

2.2. Surface Compositions of the Uranian Satellites

Classical moons. Ground-based, NIR telescope observations (~1–2.5 μm) determined that the classical moons have surface compositions dominated by a mixture of H_2O ice and a dark,
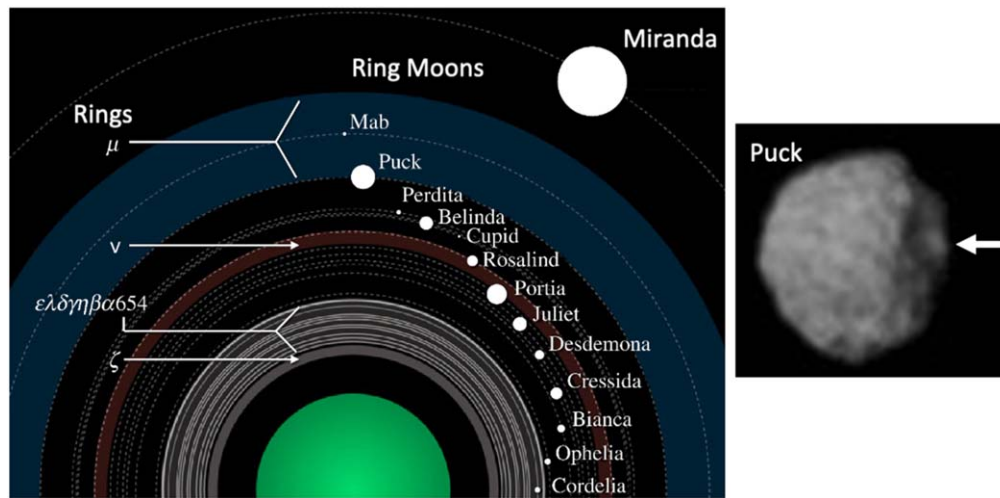
Figure 3. Left: diagram illustrating Uranus's densely packed ring and ring-moon system (modified from Showalter 2020). The sizes of the moons (white filled circles) are scaled correctly relative to each other but have been increased by a factor of 40 relative to the size of Uranus (green filled circle). Right: Voyager 2/ISS image of Puck (reprocessed by Stryk & Stooke 2008). The white arrow highlights Bogle crater, the largest crater on Puck (∼47 km diameter). Puck's south pole is located near the center of the left-side of the image.

Table 3
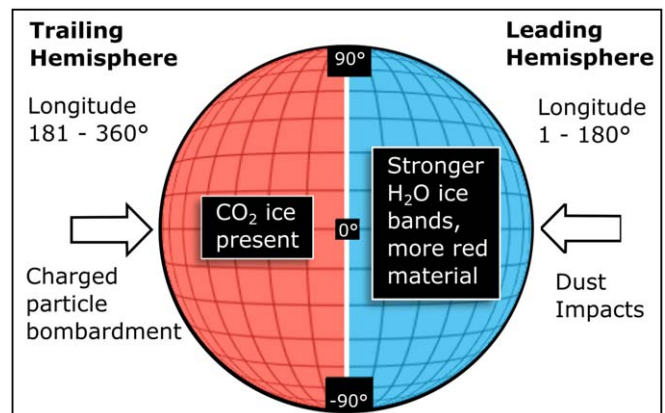Ring Moons and Irregular Satellites of Uranus

Satellites	[a]Semimajor Axis (10^5 km)	[a]Mean Radius (km)	Possible Surface Constituents
Ring Moons			
Cordelia	0.498 0	20.1 ± 3	
Ophelia	0.538 0	21.4 ± 4	
Bianca	0.592 0	27 ± 2	
Cressida	0.618 0	41 ± 2	
Desdemona	0.627 0	35 ± 4	
Juliet	0.644 0	53 ± 4	H_2O ice,
Portia	0.661 0	70 ± 4	[b]organics,
Rosalind	0.699 0	36 ± 6	[b]hydrated silicates
Cupid	0.743 9	9 ± 1	
Belinda	0.753 0	45 ± 8	
Perdita	0.764 2	13 ± 1	
Puck	0.860 0	81 ± 2	
Mab	0.977 4	6–12	
Irregular Satellites			
Francisco	42.83	11	
Caliban	72.31	36	
Stephano	80.07	16	
Trinculo	85.05	9	H_2O ice,
Sycorax	121.8	75	[b]organics,
Margaret	141.5	10	[b]hydrated silicates
Prospero	162.8	25	
Setebos	174.2	24	
Ferdinand	204.3	10	

Notes.
[a] Semimajor axis and mean radius values from the Jet Propulsion Laboratory Horizons On-Line Ephemeris System and references therein (https://ssd.jpl.nasa.gov/?sat_elem). Radius range for Mab reported in Showalter & Lissauer (2006).
[b] Possibly contributing to the ubiquitous dark material, as well as the spectrally red material detected on the irregular satellites.

Figure 4. Diagram showing the broad leading/trailing hemispherical trends in composition exhibited by Ariel, Umbriel, Titania, and Oberon, possibly driven by charged particle interactions (primarily with their trailing hemispheres) and heliocentric and planetocentric dust impacts (primarily with their leading hemispheres).

spectrally neutral material of unknown origin (e.g., Cruikshank et al. 1977; Brown & Cruikshank 1983; Brown & Clark 1984). Laboratory experiments indicate that the dark material has a spectral signature similar to amorphous carbon and/or silicates (Clark & Lucey 1984). More recent NIR telescope observations have determined that the Uranian moons display leading/trailing and planetocentric asymmetries in their compositions (Figure 4). For example, "pure" CO_2 ice (i.e., segregated from other constituents in concentrated deposits) has been detected on the trailing hemispheres of Ariel, Umbriel, Titania, and Oberon, with larger abundances on the inner moons, Ariel and Umbriel, compared with the outer moons, Titania and Oberon (Figure 5) (Grundy et al. 2003, 2006; Cartwright et al. 2015). CO_2 ice on these moons could be generated via irradiation of native H_2O ice and C-rich material by magnetospheric charged particles (Grundy et al. 2006; Cartwright et al. 2015). Supporting this hypothesis, trapped OH has possibly been detected on these moons (Roush et al. 1997), which is a strong catalyst for radiolytic generation of CO_2 molecules from substrates composed of H_2O ice and carbon-rich species (e.g., Mennella et al. 2004; Raut et al. 2012).

H_2O ice bands are weaker on the trailing hemispheres of these moons (Figure 5), perhaps in part due to large deposits of CO_2 ice masking the NIR spectral signature (∼1–2.5 μm) of H_2O ice (Cartwright et al. 2015, 2020b). Another possibility is
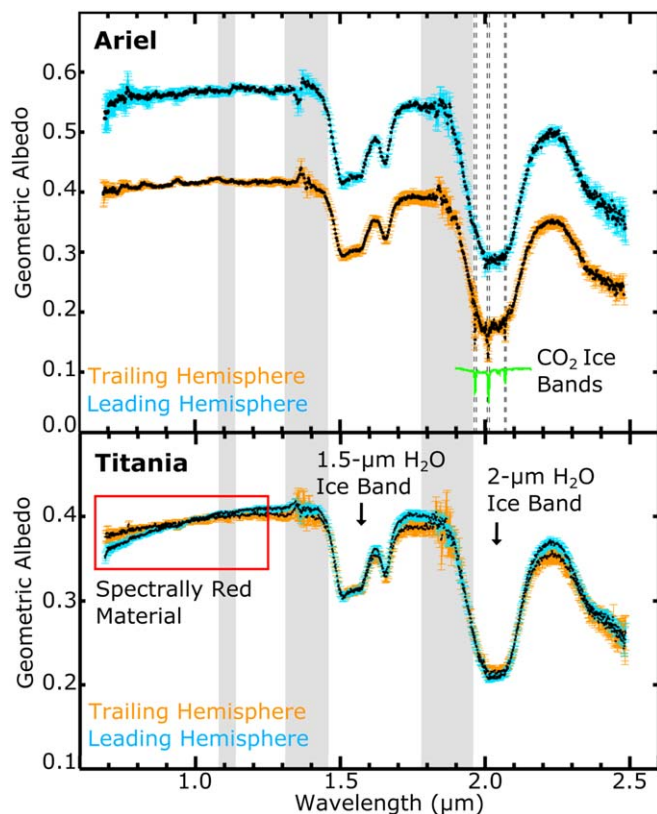
Figure 5. Top: example NIR spectra of Ariel's leading and trailing hemisphere (blue and orange 1σ error bars, respectively), collected with the SpeX Spectrograph on NASA's Infrared Telescope Facility (IRTF; Rayner et al. 2003), offset vertically for clarity. These data demonstrate the strong leading/trailing longitudinal asymmetry in the distribution of CO_2 ice observed on these moons (wavelength positions of prominent CO_2 bands are indicated with black dashed lines). The observed CO_2 ice bands are compared with an example laboratory spectrum of "pure" CO_2 ice (green) (Hansen 1997). Bottom: example IRTF/SpeX spectra of Titania's leading and trailing hemisphere (blue and orange 1σ error bars, respectively). These data highlight the NIR wavelength region where spectrally red material has been detected on these moons (0.7–1.25 μm, red box), with more red material on their leading hemispheres. These data also show the leading/trailing longitudinal asymmetry in H_2O ice band strengths, which are stronger on the leading hemispheres of Ariel, Umbriel, Titania, and Oberon. Gray shaded zones represent wavelength regions with lower atmospheric transparency and increased telluric contamination.

that heliocentric dust impacts promote regolith overturn and expose fresher H_2O ice, primarily on these moons' leading hemispheres (Cartwright et al. 2018). Spectrally red material ($\sim$0.4–1.25 μm) has also been detected, primarily on the leading hemispheres of the outer moons, Titania and Oberon (Figure 5) (Buratti & Mosher 1991; Bell & McCord 1991; Helfenstein et al. 1991; Cartwright et al. 2018). The distribution of red material could result from the accumulation of infalling planetocentric dust from retrograde irregular satellites (Buratti & Mosher 1991; Tamayo et al. 2013; Cartwright et al. 2018), which are spectrally redder than the classical moons (e.g., Grav et al. 2004; Maris et al. 2007).

Over longer wavelengths ($\sim$3–6.5 μm), spectrophotometric data collected by the Infrared Array Camera (Fazio et al. 2004) on the Spitzer Space Telescope (Werner et al. 2004) indicate that the spectral signature of CO_2 ice is strangely absent from all of these moons (Cartwright et al. 2015, 2020b). One possible explanation is that the regoliths of the classical moons are mantled by a thin layer of small H_2O ice grains ($\leqslant$2 μm

diameters), which obscures the longer wavelength spectral signature of CO_2 ice retained beneath this topmost layer (Cartwright et al. 2015, 2018, 2020b). Supporting this possibility, visible wavelength polarimetry data suggest that these moons have porous regoliths, dominated by small grains (Afanasiev et al. 2014). Similarly, over longer mid-infrared wavelengths (20–50 μm), data collected by the Infrared Interferometer Spectrometer (IRIS) on Voyager 2 suggest that Miranda and Ariel have regoliths with unusual microstructures, possibly dominated by dark, isotropically scattering grains (Hanel et al. 1986). These different data sets all suggest that the regoliths of the Uranian moons are notably different from both H_2O ice-rich and dark material-rich Galilean and Saturnian moons and may be more comparable to H_2O ice-rich trans-Neptunian objects (Afanasiev et al. 2014; Cartwright et al. 2020b; Detre et al. 2020).

Although these results are intriguing, new spacecraft measurements are needed to better understand the processes modifying the surface compositions of the Uranian moons. For example, the distribution of CO_2 ice is only longitudinally constrained, limiting our ability to determine whether this volatile is generated by charged particle radiolysis, or whether it is a native constituent sourced from their interiors. Unlike the other classical moons, CO_2 ice and leading/trailing longitudinal asymmetries in composition are absent on Miranda (Bauer et al. 2002; Grundy et al. 2006; Gourgeot et al. 2014; Cartwright et al. 2018, 2020b; DeColibus et al. 2020), adding to the mystery surrounding this moon. Because of the large obliquity of the Uranian system, and the associated seasonal effects, CO_2 ice exposed or generated at polar latitudes on these moons should sublimate, migrate in tenuous exospheres to their low latitudes, and condense in cold traps (Grundy et al. 2006; Sori et al. 2017; Cartwright et al. 2021). Spatially resolved spectra collected by an orbiter are needed to more completely understand the origin and nature of CO_2 ice. Additionally, the regolith properties of the classical moons could result from interactions with the surrounding space environment, which cannot be properly assessed without data collected by an orbiter.

Some ground-based spectra of the classical moons show a 2.2 μm absorption band (Figure 6) (e.g., Bauer et al. 2002; Cartwright et al. 2018, 2020c), which is similar to a 2.2 μm feature attributed to NH_3 and NH_4-bearing species on Pluto and its moons (e.g., Brown & Calvin 2000; Grundy et al. 2016; Cook et al. 2018; Dalle Ore et al. 2019; Cruikshank et al. 2019; Protopapa et al. 2020) and the Saturnian moon Enceladus (Emery et al. 2005; Verbiscer et al. 2006). NH_3 and NH_4 are highly efficient anti-freeze agents when mixed with liquid H_2O that could promote the retention of subsurface oceans if present within the interiors of these moons (e.g., Spohn & Schubert 2003; Hussmann et al. 2015; Nimmo & Pappalardo 2016). Because NH_3-rich planetesimals were likely incorporated into the proto-Uranian moons as they formed in the Uranian subnebula (e.g., Lewis 1972), large quantities of NH_3 could be present in their interiors. Furthermore, unlike H_2O ice and CO_2 ice, the 2.2 μm band does not display leading/trailing longitudinal asymmetries in its distribution (Figure 6), which suggests that NH_3-bearing and NH_4-bearing species are native to these moons and are exposed by impact events, tectonism, and mass wasting, and/or emplaced in cryovolcanic deposits (Cartwright et al. 2020c). Other species like carbonates (-CO_3 group), including ammonium carbonate ((NH_4)$_2CO_3$), could be
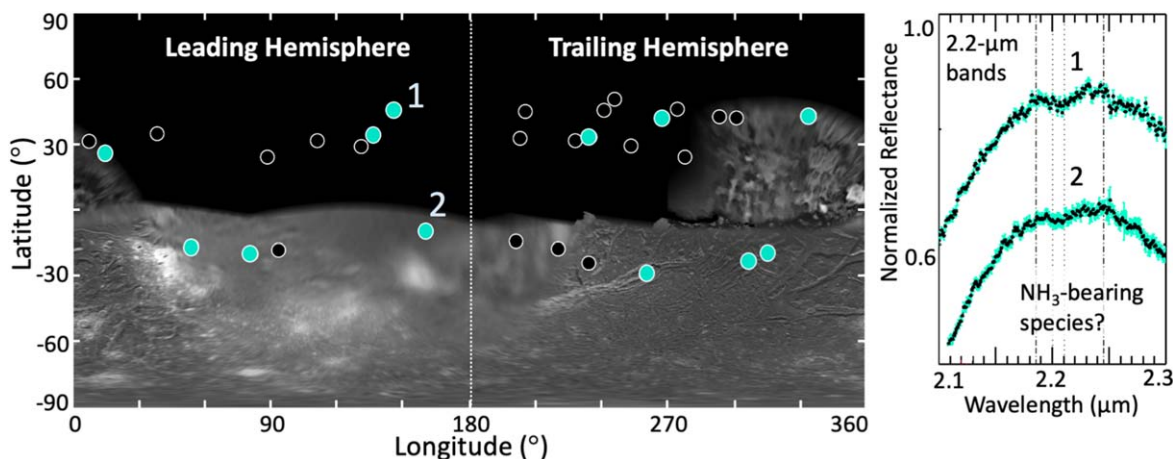
Figure 6. Left: Mercator map projection of Voyager 2/ISS images of Ariel (courtesy NASA/JPL/Caltech/USGS, reprocessed by Stryk & Stooke 2008). The cyan dots represent the mid-observation longitude and latitude for ground-based spectra that show 2.2 μm bands, and the black dots represent spectra that do not display 2.2 μm bands (modified from Cartwright et al. 2020c). These spectra are disk-integrated and average over an entire hemisphere of Ariel. Spectra for the dots labeled "1" and "2" are shown on the right. Right: example IRTF/SpeX spectra of Ariel that display 2.2 μm bands, offset vertically for clarity. Dotted–dashed lines highlight the wavelength range of the 2.2 μm band, and the dotted lines highlight the wavelength range of its band center.

contributing to the 2.2 μm band as well (Cartwright et al. 2020c). Higher spatial resolution spectra are needed to measure the spectral signature and spatial distribution of the 2.2 μm band to determine whether these moons are rich in NH_3 and other species that may have been sourced from liquid layers in their interiors.

The composition and origin of the widespread dark material and the spectrally red material on the Uranian moons remains poorly understood. These materials could be rich in hydrated silicates and organic constituents delivered to and/or native to these moons. Prior spacecraft missions have assessed the nature of organics in the Jupiter, Saturn, and Pluto systems, as well as on comets (e.g., McCord et al. 1997; Irvine et al. 2003; Clark et al. 2005; Waite et al. 2009; Capaccioni et al. 2015; Grundy et al. 2016; Cruikshank et al. 2020). Measuring the spectral signature of organics (e.g., C-H stretching modes between 3.2 and 3.5 μm) in the Uranian system represents a key heliocentric link for improving our understanding of the nature and overall distribution of organic matter in the solar system, as well as for investigating whether organics formed within the protoplanetary disk or were delivered as interstellar matter. Thus, new measurements made by an orbiter are critical for determining the spatial distribution and spectral signature of CO_2 ice and NH_3-bearing species on the classical moons, and whether these constituents were exposed/emplaced on their surfaces by ocean world activity, as well as for investigating the origin and evolution of organic material in the Uranian System.

Ring moons and irregular satellites. Far less is known about the compositions of Uranus smaller ring moons and irregular satellites, which are too faint for spectroscopic observations using available telescopes (apparent magnitudes ranging between 19.8 and 25.8 at visible wavelengths). Photometric data sets indicate that the ring moons are dark (except possibly Mab, Showalter & Lissauer 2006), with neutral spectral slopes and slight reductions in albedo at 1.5 and 2.0 μm, consistent with the presence of H_2O ice (e.g., Karkoschka 2001). More recent photometric measurements indicate that the ring moons may display latitudinal variations in albedo, possibly resulting from interactions with Uranus's magnetosphere (Paradis et al. 2019). Other photometric studies determined that Uranus's irregular satellites are dark and red (e.g., Grav et al. 2004;

Maris et al. 2007), with possibly redder colors than the irregular satellites of the other giant planets (Graykowski & Jewitt 2018). Spectra of the largest Uranian irregular satellite Sycorax suggest that H_2O ice is present (Romon et al. 2001), but no spectra exist for the other, fainter irregular satellites. Therefore, the compositions of these objects are essentially unknown, and new observations made by an orbiter are needed.

3. Conclusions and Recommendations for Future Exploration

Data returned by Voyager 2 and ground- and space-based telescopes have revealed tantalizing glimpses of the Uranian moons' geologic histories, compositions, and interactions with the surrounding space environment. However, Uranus's 27 satellites remain poorly understood. Only six Uranian moons were spatially resolved by ISS, and the flyby nature of the Voyager 2 encounter, the lack of a VIS/NIR mapping spectrometer, and the low spatial resolution of collected data sets left many unanswered questions and limit our ability to determine whether the classical moons are, or were, ocean worlds. Future telescope facilities like the Extremely Large Telescopes (ELTs) and the proposed Large UV/Optical/IR Surveyor (LUVOIR) space telescope (e.g., Roberge et al. 2019) will be able to collect high quality images and spectra of the classical moons (Cartwright et al. 2019; Wong et al. 2020), providing new information about their surfaces (Figure 7). Although these telescope data sets will undoubtedly increase our knowledge of these moons, they will not be able to achieve sufficient spatial resolutions to identify linkages between geologic features and their surface compositions, nor probe their internal structures, or investigate moon-magnetosphere interactions (e.g., Kollmann et al. 2020). Furthermore, these telescope data sets will not be able to spatially resolve the ring moons and irregular satellites to assess their surface geologies and origins.

An orbiting spacecraft equipped with a magnetometer could search for induced magnetic fields emanating from briny oceans in the interiors of the classical moons. An orbiter could also search for plumes on the classical moons and other signs of recent endogenic geologic activity. An orbiter making multiple close flybys of Uranus's rings would dramatically
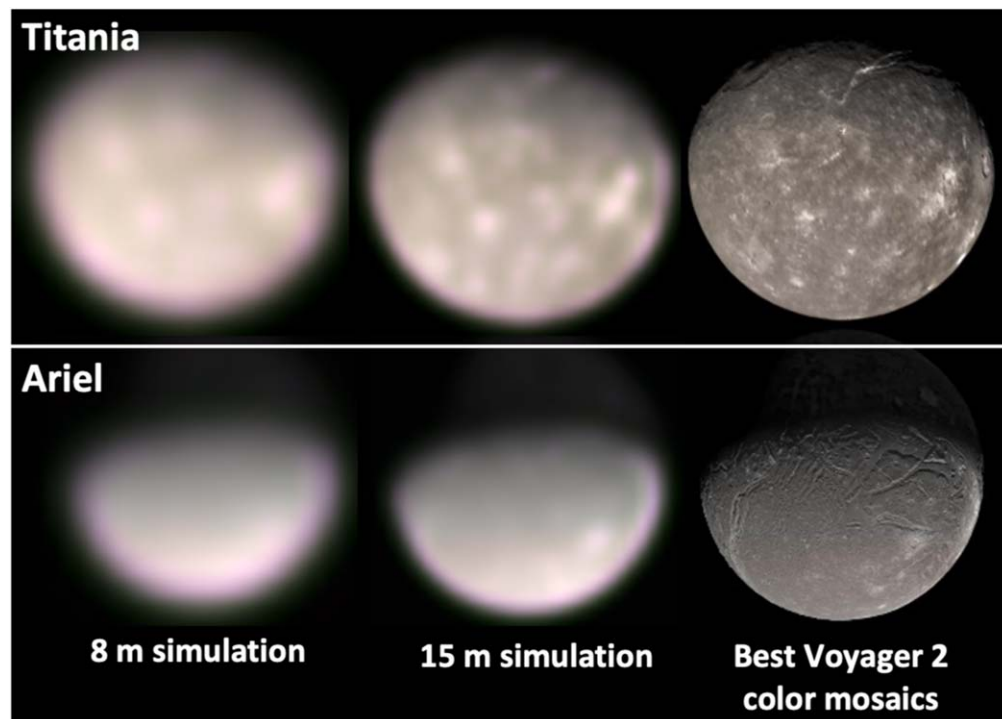
Figure 7. Resampled and real images of Titania and Ariel. Real images (right) are Voyager 2/ISS image mosaics (courtesy NASA/JPL/Caltech/USGS, reprocessed by Stryk & Stooke (2008)). Resampled images simulate what these moons would look like as seen by LUVOIR from the Earth-Sun L2 Lagrange point in 2040 with an 8 m (left) and 15 m (center) aperture. The simulated angular diameters are $\sim0.''08$ and $\sim0.''12$ for Ariel and Titania, respectively.

improve our understanding of the ring moons and could investigate whether Mab is the source of the μ-ring. An orbiter could spend time looking outward, making key observations of the distant irregular satellites, similar to Cassini's observations of Saturn's irregular satellites (Denk & Mottola 2019). A close pass of an irregular satellite inbound to Uranus, like Cassini's inbound flyby of Phoebe (Porco et al. 2005), would represent an unparalleled opportunity to investigate the nature and origin of these likely captured objects. Thus, new data sets collected by an orbiter are essential for improving our understanding of the icy residents of the Uranian system and determining whether Uranus's five classical moons are, or were, ocean worlds.

ORCID iDs

Richard J. Cartwright https://orcid.org/0000-0002-6886-6009
Chloe B. Beddingfield https://orcid.org/0000-0001-5048-6254
Tom A. Nordheim https://orcid.org/0000-0001-5888-4636
Catherine M. Elder https://orcid.org/0000-0002-9993-8861
Julie C. Castillo-Rogez https://orcid.org/0000-0003-0400-1038
Marc Neveu https://orcid.org/0000-0002-6220-2869
Ali M. Bramson https://orcid.org/0000-0003-4903-0916
Michael M. Sori https://orcid.org/0000-0002-6191-2447
Bonnie J. Buratti https://orcid.org/0000-0002-5901-4875
Robert T. Pappalardo https://orcid.org/0000-0003-2571-4627
Joseph E. Roser https://orcid.org/0000-0002-1806-3494
Ian J. Cohen https://orcid.org/0000-0002-9163-6009
Erin J. Leonard https://orcid.org/0000-0002-5150-5426
Anton I. Ermakov https://orcid.org/0000-0002-7020-7061
Mark R. Showalter https://orcid.org/0000-0002-8580-4053
William M. Grundy https://orcid.org/0000-0002-8296-6540
Elizabeth P. Turtle https://orcid.org/0000-0003-1423-5751
Mark D. Hofstadter https://orcid.org/0000-0002-3208-3918

References

Afanasiev, V., Rosenbush, V., & Kiselev, N. 2014, AstBu, 69, 211
Bauer, J. M., Roush, T. L., Geballe, T. R., et al. 2002, Icar, 158, 178
Beddingfield, C., Burr, D., & Emery, J. 2015, Icar, 247, 35
Beddingfield, C., Li, C., Atreya, S., et al. 2020a, arXiv:2007.11063
Beddingfield, C. B., & Cartwright, R. J. 2020b, Icar, 343, 113687
Beddingfield, C. B., & Cartwright, R. J. 2021, Icar, in press (doi:10.1016/j.icarus.2021.114583)
Bell, J., III, & McCord, T. 1991, LPSC, 21, 473
Brown, M. E., & Calvin, W. M. 2000, Sci, 287, 107
Brown, R. H., & Clark, R. N. 1984, Icar, 58, 288
Brown, R. H., & Cruikshank, D. P. 1983, Icar, 55, 83
Buratti, B. J., & Mosher, J. A. 1991, Icar, 90, 1
Capaccioni, F., Coradini, A., Filacchione, G., et al. 2015, Sci, 347, aaa0628
Cartwright, R., Beddingfield, C., Showalter, M., Cruikshank, D., & Nordheim, T. 2020a, LPSC, 51, 1699
Cartwright, R., Nordheim, T., Grundy, W., et al. 2021, LPSC, 52, 1298

Cartwright, R. J., Beddingfield, C. B., Nordheim, T. A., et al. 2020c, ApJL, 898, L22
Cartwright, R. J., Emery, J. P., Grundy, W. M., et al. 2020b, Icar, 338, 113513
Cartwright, R. J., Emery, J. P., Pinilla-Alonso, N., et al. 2018, Icar, 314, 210
Cartwright, R. J., Emery, J. P., Rivkin, A. S., Trilling, D. E., & Pinilla-Alonso, N. 2015, Icar, 257, 428
Cartwright, R. J., Holler, B., Benecchi, S., et al. 2019, BAAS, 51, 132
Clark, R. N., Brown, R. H., Jaumann, R., et al. 2005, Natur, 435, 66
Clark, R. N., & Lucey, P. G. 1984, JGR, 89, 6341
Cochrane, C., Nordheim, T., Vance, S., et al. 2021, LPSC, 52, 1559
Cohen, I., Beddingfield, C., Chancia, R., et al. 2020, LPSC, 51, 1428
Cook, J. C., Dalle Ore, C. M., Protopapa, S., et al. 2018, Icar, 315, 30
Croft, S. 1987, LPSC, 18, 207
Croft, S., & Soderblom, L. 1991, Uranus (Tucson, AZ: Univ. Arizona Press), 561
Cruikshank, D., Pilcher, C. B., & Morrison, D. 1977, ApJ, 217, 1006
Cruikshank, D. P. 1980, Icar, 41, 246
Cruikshank, D. P., & Brown, R. H. 1981, Icar, 45, 607
Cruikshank, D. P., Pendleton, Y. J., & Grundy, W. M. 2020, Life, 10, 126
Cruikshank, D. P., Umurhan, O. M., Beyer, R. A., et al. 2019, Icar, 330, 155
Ćuk, M., El Moutamid, M., & Tiscareno, M. S. 2020, PSJ, 1, 22
Dalle Ore, C., Cruikshank, D., Protopapa, S., et al. 2019, SciA, 5, eaav5731
De Pater, I., Hammel, H. B., Gibbard, S. G., & Showalter, M. R. 2006, Sci, 312, 92
DeColibus, D., Chanover, N., & Cartwright, R. 2020, AAS/DPS Meeting, 52, 215
Denk, T., & Mottola, S. 2019, Icar, 322, 80
Detre, Ö, Müller, T., Klaas, U., et al. 2020, A&A, 641, A76
Emery, J., Burr, D., Cruikshank, D., Brown, R. H., & Dalton, J. 2005, A&A, 435, 353
Fazio, G., Hora, J., Allen, L., et al. 2004, ApJS, 154, 10
Fletcher, L. N., Helled, R., Roussos, E., et al. 2020, P&SS, 191, 105030
French, R. S., Showalter, M. R., de Pater, I., & Lissauer, J. J. 2017, AAS/DPS Meeting, 49, 214.19
Gladman, B., Kavelaars, J., Holman, M., et al. 2000, Icar, 147, 320
Gladman, B. J., Nicholson, P. D., Burns, J. A., et al. 1998, Natur, 392, 897
Gourgeot, F., Dumas, C., Merlin, F., Vernazza, P., & Alvarez-Candal, A. 2014, A&A, 562, A46
Grav, T., Holman, M. J., & Fraser, W. C. 2004, ApJL, 613, L77
Graykowski, A., & Jewitt, D. 2018, AJ, 155, 184
Greenberg, R. J., Croft, S. K., Janes, D. M., et al. 1991, Uranus (Tucson, AZ: Univ. Arizona Press), 693
Grundy, W., Binzel, R., Buratti, B., et al. 2016, Sci, 351, aad9189
Grundy, W., Young, L., Spencer, J., et al. 2006, Icar, 184, 543
Grundy, W., Young, L., & Young, E. 2003, Icar, 162, 222
Hammond, N. P., & Barr, A. C. 2014, Geo, 42, 931
Hanel, R., Conrath, B., Flasar, F., et al. 1986, Sci, 233, 70
Hansen, G. B. 1997, AdSpR, 20, 1613
Helfenstein, P., Hillier, J., Weitz, C., & Veverka, J. 1991, Icar, 90, 14
Helfenstein, P., Thomas, P. C., & Veverka, J. 1989, Natur, 338, 324
Hendrix, A. R., Hurford, T. A., Barge, L. M., et al. 2019, AsBio, 19, 1
Hofstadter, M., Simon, A., Atreya, S., et al. 2019, P&SS, 177, 104680
Hussmann, H., Sotin, C., & Lunine, J. 2015, Treatise on Geophysics: Second Edition, Vol. 10 (Amsterdam: Elsevier), 605
Irvine, W. M., Bergman, P., Lowe, T. B., et al. 2003, OLEB, 33, 609

Jacobson, R., Campbell, J., Taylor, A., & Synnott, S. 1992, AJ, 103, 2068
Jewitt, D., & Haghighipour, N. 2007, ARA&A, 45, 261
Kargel, J. 1995, in Comparative Planetology with an Earth Perspective (Berlin: Springer), 101
Karkoschka, E. 2001, Icar, 151, 51
Kavelaars, J., Holman, M., Grav, T., et al. 2004, Icar, 169, 474
Kirchoff, M. R., & Schenk, P. 2009, Icar, 202, 656
Kollmann, P., Cohen, I., Allen, R., et al. 2020, SSRv, 216, 1
Leonard, E., Elder, C., Nordheim, T., et al. 2021, PSJ, submitted
Lewis, J. S. 1972, E&PSL, 15, 286
Maris, M., Carraro, G., & Parisi, M. G. 2007, A&A, 472, 311
McCord, T. a., Carlson, R., Smythe, W., et al. 1997, Sci, 278, 271
McKinnon, W. B., Chapman, C. R., & Housen, K. R. 1991, Uranus (Tucson, AZ: Univ. Arizona Press), 629
Mennella, V., Palumbo, M., & Baratta, G. 2004, ApJ, 615, 1073
Moore, J. M., Schenk, P. M., Bruesch, L. S., Asphaug, E., & McKinnon, W. B. 2004, Icar, 171, 421
Nimmo, F., & Pappalardo, R. 2016, JGRE, 121, 1378
Pappalardo, R. T., Reynolds, S. J., & Greeley, R. 1997, JGR, 102, 13369
Paradis, S., Moeckel, C., Tollefson, J., & de Pater, I. 2019, AJ, 158, 178
Peterson, G., Nimmo, F., & Schenk, P. 2015, Icar, 250, 116
Plescia, J. 1987, Natur, 327, 201
Porco, C., Baker, E., Barbara, J., et al. 2005, Sci, 307, 1237
Protopapa, S., Cook, J., Grundy, W., et al. 2020, Pluto System after New Horizons (Tucson, AZ: Univ. Arizona Press)
Raut, U., Fulvio, D., Loeffler, M., & Baragiola, R. 2012, ApJ, 752, 159
Rayner, J., Toomey, D., Onaka, P., et al. 2003, PASP, 115, 362
Roberge, A., Bolcar, M. R., & France, K. C. 2019, Proc. SPIE, 11115, 111150O
Romon, J., De Bergh, C., Barucci, M., et al. 2001, A&A, 376, 310
Roush, T., Noll, K., Cruikshank, D., & Pendleton, Y. 1997, AAS/DPS Meeting, 29, 20.03
Schenk, P. M. 1991, JGR, 96, 1887
Schenk, P. M., & Moore, J. M. 2020, RSPTA, 378, 20200102
Sfair, R., & Winter, S. G. 2012, A&A, 543, A17
Sheppard, S. S., Jewitt, D., & Kleyna, J. 2005, AJ, 129, 518
Showalter, M. R. 2020, RSPTA, 378, 20190482
Showalter, M. R., & Lissauer, J. J. 2006, Sci, 311, 973
Smith, B. A., Soderblom, L., Beebe, R., et al. 1986, Sci, 233, 43
Soifer, B., Neugebauer, G., & Matthews, K. 1981, Icar, 45, 612
Sori, M. M., Bapst, J., Bramson, A. M., Byrne, S., & Landis, M. E. 2017, Icar, 290, 1
Spohn, T., & Schubert, G. 2003, Icar, 161, 456
Steinbrügge, G., Steinke, T., Thor, R., Stark, A., & Hussmann, H. 2019, Geosc, 9, 320
Stryk, T., & Stooke, P. 2008, LPSC, 39, 1362
Tamayo, D., Burns, J. A., & Hamilton, D. P. 2013, Icar, 226, 655
Tittemore, W. C., & Wisdom, J. 1990, Icar, 85, 394
Verbiscer, A. J., Peterson, D. E., Skrutskie, M. F., et al. 2006, Icar, 182, 211
Waite, J. H., Jr, Lewis, W., Magee, B., et al. 2009, Natur, 460, 487
Weiss, B., Biersteker, J., Colicci, V., et al. 2021, LPSC, 52, 2096
Werner, M. W., Roellig, T., Low, F., et al. 2004, ApJS, 154, 1
Wong, M. H., Meech, K. J., Dickinson, M., et al. 2020, arXiv:2009.08029
Zahnle, K., Schenk, P., Levison, H., & Dones, L. 2003, Icar, 163, 263